Acute degradation reveals that Ran-Importin network dynamically polarizes and maintains HURP, but not NuMA, on human mitotic spindle

Kenta Tsuchiya[1#], Hisato Hayashi[1#], Momoko Nishina[1#], Masako Okumura[1#], Masato T. Kanemaki[2,3], Gohta Goshima[1], Tomomi Kiyomitsu[1,2*]

[1] Division of Biological Science, Graduate School of Science, Nagoya University, Chikusa-ku, Nagoya 464-8602, Japan.

[2] Precursory Research for Embryonic Science and Technology (PRESTO) Program, Japan Science and Technology Agency, 4-1-8 Honcho Kawaguchi, Saitama 332-0012, Japan.

[3] Department of Chromosome Science, National Institute of Genetics, Research Organization of Information and Systems (ROIS), and Department of Genetics, SOKENDAI (The Graduate University of Advanced Studies), Yata 1111, Mishima, Shizuoka 411-8540, Japan.

# These authors contributed equally to this work.

* Corresponding author:

E-mail: kiyomitsu@bio.nagoya-u.ac.jp

Phone & Fax: +81-52-789-2938

Characters: 25,699 characters

Abstract

The chromosome-derived Ran-GTP gradient is believed to promote spindle assembly by releasing spindle assembly factors (SAFs) such as NuMA and HURP from inhibitory importins near chromosomes. The Ran-GTP gradient plays critical roles in meiosis, but how the Ran-based network spatiotemporally defines SAF localization and function in mitosis remains incompletely understood. Here, we systematically depleted RCC1 (Ran-GEF), RanGAP1, and importin-β using auxin-inducible degron (AID) technology in somatic human cells. We demonstrate that the Ran-Importin network does not substantially affect NuMA localization and functions at spindle poles. In contrast, the Ran-based network polarizes both HURP and importin-β on K-fibers near chromosomes, where HURP, but not importin-β, stabilizes microtubules. In addition, acute RCC1 degradation during metaphase reveals that HURP's K-fiber localization is dynamically maintained by Ran-GTP even after spindle assembly. Together, we propose that the Ran-Importin network locally promotes microtubule-binding and dissociation cycle of HURP, but not NuMA, to dynamically organize stable K-fibers near chromosomes in mitotic human cells.

41 **A condensed title** (50 characters)

42 Ran-based polarization of SAFs on human mitotic spindle

43

44

45 **Summary** (40 words)

46 Using auxin-inducible degron technology, we systematically analyzed the mechanisms
47 of Ran-based polarization of spindle assembly factors on human mitotic spindles. We
48 find that the Ran-based network dynamically polarizes and maintains HURP, but not
49 NuMA, by promoting local microtubule binding-dissociation cycle.
50 (40 words)

51

52

53 **Highlights**

54 • Ran-GTP is dispensable for NuMA localization and function at spindle poles in mitotic
55 human cells.
56 • Ran-Importin network is indispensable for HURP and importin-β to accumulate at K-
57 fibers near chromosomes.
58 • HURP, but not importin-β, is required to stabilize K-fibers.
59 • HURP is dynamically maintained on K-fibers even after spindle assembly.

60

Introduction

To achieve accurate capture and segregation of chromosomes by spindle microtubules, chromosomes generate intracellular gradients that promote spindle assembly near chromosomes in both mitosis and meiosis (Heald and Khodjakov, 2015; Kalab and Heald, 2008). During animal mitosis, the chromosome-derived gradients and centrosome-dependent pathways coordinately regulate microtubule nucleation, polymerization/depolymerization, transport, sliding, and cross-linking to organize bipolar spindle structure (Goshima and Scholey, 2010; Petry, 2016; Walczak and Heald, 2008). In contrast, chromosome-derived signals play particularly dominant roles in spindle assembly during female meiosis as centrosomes are absent (Beaven et al., 2017; Bennabi et al., 2016; Mogessie et al., 2018).

Chromosome-derived signals consist of two distinct pathways - the Ran-GTP gradient and chromosome passenger complex (CPC)-based signals (Zierhut and Funabiki, 2015). The Ran-GTP gradient is generated by two spatially-separated opposing enzymes. Regulator of chromosome condensation 1 (RCC1), is a guanine nucleotide exchange factor (GEF) for Ran (Bischoff and Ponstingl, 1991) and localizes to chromosomes to convert the small GTPase Ran from its GDP- to GTP-bound form (Moore et al., 2002) (Fig. 1A). In contrast, RanGAP1, a GTPase-activating protein (GAP) for Ran, predominantly localizes to the cytoplasm to promote Ran's intrinsic GTPase activity (Bischoff et al., 1994) (Fig. 1A). The Ran-GTP gradient has been best characterized in meiotic *Xenopus* egg extracts, but is also found in other meiotic and mitotic cell types (Dumont et al., 2007; Hasegawa et al., 2013; Kalab et al., 2006; Moutinho-Pereira et al., 2013).

Pioneering work using *Xenopus* egg extracts established a model in which a chromosome-derived Ran-GTP gradient promotes spindle assembly by activating spindle assembly factors (SAFs) such as NuMA and TPX2 by releasing them from inhibitory importin proteins in the vicinity of chromosomes (Fig.1A) (Kalab and Heald, 2008; Nachury et al., 2001; Wiese et al., 2001). At present, several other microtubule-binding proteins, such as HURP (Sillje et al., 2006), have been identified as spindle assembly factors that promote spindle assembly downstream of Ran-GTP gradient (Forbes et al., 2015). In addition to a role in spindle assembly, we previously demonstrated that the Ran-GTP gradient promotes spindle positioning by controlling the spatial organization of cortical proteins such as NuMA-LGN complex and Anillin in somatic human cells (Kiyomitsu and Cheeseman, 2012; Kiyomitsu and Cheeseman, 2013).

In mitotic human cells, NuMA localizes to spindle poles and the cell cortex, where NuMA acts for spindle-pole focusing and astral microtubule capture/pulling, respectively, in cooperation with a microtubule motor dynein (Hueschen et al., 2017; Kiyomitsu, 2019; Okumura et al., 2018). Although the mechanisms remain unclear, cortical localization of NuMA-LGN complexes is negatively regulated by the chromosome-derived Ran-GTP gradient in a distance dependent manner (Kiyomitsu and Cheeseman, 2012). Similarly, NuMA is excluded from spindle microtubules near chromosomes, and accumulates around spindle poles. How Ran-GTP regulates the spindle localization of NuMA is also mysterious, but recent structural and *in vitro* studies demonstrated that importin-α/β recognizes nuclear localization signal (NLS) of NuMA, and sterically inhibits NuMA's 2nd microtubule-binding domain (Chang et al., 2017). The

107 authors predicted that NuMA would be liberated from importin-β near chromosomes by
108 Ran-GTP gradient and subsequently acts for spindle assembly (Chang et al., 2017).
109 However, this model has not been rigorously tested with cell biological approaches. In
110 addition, the significance of the Ran-GTP gradient for mitotic spindle assembly has
111 been debated and appears to vary across cell types (Furuta et al., 2016; Hasegawa et
112 al., 2013; Moutinho-Pereira et al., 2013).

113 To define the significance and mechanisms of Ran-based spindle assembly in
114 mitotic cells, we sought to systematically deplete Ran-associated proteins in mitotic
115 human cells using auxin-inducible degron (AID) technology (Natsume et al., 2016). We
116 found that degradation of the Ran-based network does not substantially affect NuMA
117 localization or function at spindle poles. In sharp contrast, Ran-GTP polarizes both
118 HURP and importin-β on kinetochore-fibers (K-fibers) near chromosomes, where HURP
119 and importin-β have distinct roles in K-fiber stabilization. Furthermore, we first
120 demonstrated that HURP is dynamically maintained on K-fibers after spindle assembly.
121 Based on our findings, we propose a local cycling model in which the Ran-based
122 network promotes a local microtubule binding-dissociation cycle of HURP to
123 dynamically organize stable K-fibers near chromosomes.
124

Results

Ran-Importin network does not substantially affect spindle-pole localization of NuMA in human cells

NuMA is required for mitotic spindle assembly in mammalian cells (Gaglio et al., 1995; Hueschen et al., 2017; Okumura et al., 2018; Silk et al., 2009), and has been proposed to be regulated by Ran-GTP (Chang et al., 2017; Nachury et al., 2001; Wiese et al., 2001). However, how the chromosome-derived Ran-GTP gradient regulates NuMA's spindle-pole localization is poorly understood in mitotic human cells. To address this, we sought to systematically deplete RCC1 (RanGEF), RanGAP1, and importin-β using auxin-inducible degron (AID) technology (Fig. 1A-B) (Natsume et al., 2016). We introduced a C-terminal mAID-mClover (mAC) tag into both alleles of either RCC1, RanGAP1, or importin-β at their genomic loci (Fig. 1C-E and Fig. S1A, D, G) in parental tet-OsTIR1 HCT116 cells that conditionally express OsTIR1 following the addition of doxycycline (Dox) (Fig.1B) (Natsume et al., 2016). To visualize endogenous NuMA in living cells, we integrated an mCherry tag into both alleles of the NuMA genomic locus (Fig. 1C-E and S1B-C, E-F, H-I). As expected, RCC1-mAC accumulated on mitotic chromosomes (Fig. 1C top) (Moore et al., 2002), whereas RanGAP1-mAC localized to the cytoplasm and was excluded from chromosomes with weak accumulation at kinetochores (Fig. 1D top)(Joseph et al., 2002). NuMA-mCherry localized to the spindle poles in metaphase (Fig. 1C-E) (Compton et al., 1992; Kiyomitsu and Cheeseman, 2012). Unexpectedly, we found that endogenous importin-β-mAC was detected not only in cytoplasm, but also at the chromosome-proximal region of bundled kinetochore-microtubules (K-fibers) in living cells (Fig. 1E top, S1J). Although this contrasts with

spindle-pole localization of importin-β observed using pre-extracted fixed cells (Ciciarello et al., 2004), the K-fiber localization of importin-β was not a consequence of mAC tagging, as we observed K-fiber localization after immunostaining for endogenous importin-β (Fig. S1K).

To understand how NuMA is regulated by the Ran-Importin network (Fig. 1A), we next depleted RCC1, RanGAP1, or importin-β by treatment with Dox and auxin (IAA). After 20-24 hrs, the fluorescence intensities of mAC-tagged RCC1, RanGAP1, and importin-β were reduced to undetectable levels (Fig. 1C-E bottom), although some populations of cells still displayed fluorescent signals, likely due to heterogeneous induction of OsTIR1 (see cells with * in Fig. 1E bottom). Importantly, degradation of either RCC1, RanGAP1, or importin-β did not substantially affect the spindle-pole localization of NuMA at metaphase (Fig. 1C-E). These results indicate that the Ran-importin network is dispensable for spindle-pole localization of NuMA in cultured human cells.

NuMA acts for spindle-pole focusing independently of RCC1

NuMA depletion causes spindle-pole focusing defects in human cells (Hueschen et al., 2017; Okumura et al., 2018). Given that RCC1 depletion did not substantially affect spindle bipolarity (Fig. 1C, F), NuMA is still functional at spindle poles in the absence of RCC1. To confirm this, we next co-depleted RCC1 and NuMA. We integrated mAID-mCherry tag into both alleles of the NuMA genomic locus in the parental RCC1-mAC cell line (Fig. 1G and S1L). As expected, co-depletion of RCC1 and NuMA caused defects in spindle-pole focusing and/or bipolar spindle formation (Fig. 1F, 1G bottom,

and Fig. S1M). These results indicate that NuMA is still functional for spindle-pole focusing in the absence of Ran-GTP in mitotic human cells.

Degradation of RCC1 during prometaphase does not substantially affect localization and function of NuMA at spindle poles

NuMA is transported into the nucleus via its nuclear localization signal (NLS) during interphase (Fig. 2A, see cells with (+) (Chang et al., 2017; Tang et al., 1994). In the interphase nucleus, NuMA is likely released from importins by nuclear Ran-GTP. Because we found that NuMA is maintained in the nucleus following RCC1 degradation in interphase (Fig. 2A, see cells with (-), Fig. 2B, t = -1:35 and -0:15), this raises another possibility that the majority of NuMA is maintained as an active form free from importin-β in the nucleus and works properly in the subsequent mitosis in RCC1-depleted cells (Fig. 1). To exclude this possibility, we next depleted RCC1 in nocodazole-arrested cells and analyzed the phenotypes following nocodazole washout (Fig. 2C).

In RCC1-positive control cells, NuMA localized diffusely to the cytoplasm during nocodazole arrest (Fig. 2D, t = -90), but rapidly accumulated near chromosome masses within 10 min following nocodazole washout (Fig. 2D, t = 10). NuMA localized at the poles of metaphase spindles within 60 min (Fig. 2D, t = 60) and entered the nucleus following mitotic exit (Fig. 2D, t = 85). Following nocodazole washout, NuMA also displayed punctate foci in the cytoplasm (Fig. 2D, t = 10), which were rarely observed in normal prometaphase cells (Fig. 2A t = 0:05) and disappeared during spindle assembly (Fig. 2D, t = 60). Importantly, NuMA behaved similarly when RCC1 was degraded during nocodazole arrest. RCC1-mAC signals were detectable on chromosome masses

194 in nocodazole-arrested cells (Fig. 2E, t = -90), and were reduced to undetectable levels
195 after the addition of IAA (Fig. 4E, t = 0). NuMA accumulated near chromosome masses
196 within 10 min following nocodazole washout (Fig. 2E, t = 10), and localized to spindle
197 poles around 60 min (Fig. 2E, t = 55). Although cortical NuMA signals appeared to be
198 reduced, RCC1-depleted cells entered anaphase with similar timing (Fig. 2E, t = 70, Fig.
199 2G). In addition, even if RCC1 was degraded before the addition of IAA due to a basal
200 activity of OsTIR1 (Fig. 2F, see cells indicated by (3) at t = -90, Fig. S2A) (Yesbolatova
201 et al., 2019), there were no significant differences in timing for bipolar spindle assembly
202 and mitotic exit (Fig. 2F-G, Fig. S2A). These results indicate that RCC1 is dispensable
203 for NuMA localization and function at spindle poles even if RCC1 is degraded during
204 mitosis.

205

206 **RCC1 regulates kinetochore-fiber localization of HURP and importin-β**

207 The above results indicate that RCC1 is dispensable for localization and function of
208 NuMA at spindle poles. However, RCC1 depletion in asynchronous cultures caused
209 shorter mitotic spindle (Fig. 1C, 2A-B, 3A), suggesting that Ran-GTP plays roles for
210 proper spindle assembly in somatic human cells. To identify spindle assembly factors
211 downstream of RCC1, we next analyzed the localization of TPX2 (Gruss et al., 2001)
212 and HURP (Sillje et al., 2006), since these proteins are well-recognized as Ran-
213 regulated spindle assembly factors. TPX2 localized to spindle microtubules in
214 metaphase (Fig. 3B top). However, the localization of TPX2 was virtually unaffected in
215 RCC1-depleted cells (Fig. 3B and Fig. S3A) as observed for NuMA (Fig. 1C). In sharp
216 contrast, K-fiber accumulation of HURP was completely abolished following RCC1

depletion (Fig. 3C and Fig. S3B). HURP localized diffusely in the cytoplasm with weak accumulation on the spindle in RCC1-depleted cells (Fig. 3C). Because HURP directly interacts with importin-β (Sillje et al., 2006) and co-localized with importin-β at K-fibers (Fig. S1K), we next analyzed the localization of importin-β. As observed for HURP, the K-fiber localization of importin-β was diminished in RCC1-depleted cells (Fig. 3D and Fig. S3C). These results suggest that the chromosome-derived Ran-GTP gradient acts primarily to target HURP and importin-β near chromosomes, but not NuMA and TPX2 around spindle poles, in cultured human cells.

HURP, but not importin-β, is required to stabilize K-fibers

HURP is required to stabilize K-fibers (Sillje et al., 2006). To understand the relationship between HURP and importin-β for their K-fiber localization and function, we next targeted endogenous HURP by introducing a mAID-mClover-3xFLAG (mACF) tag (Fig. 4A and Fig. S4A-C). Endogenous HURP-mACF accumulated at K-fibers near chromosomes (Fig. 4A) as observed with anti-HURP antibodies (Sillje et al., 2006). HURP depletion resulted in diminished importin-β localization to K-fibers (Fig. 4A-B) and reduced mitotic spindle length (Fig. 4C). Because K-fibers are resistant to cold treatment (Sillje et al., 2006), we next incubated cells with ice-cold medium for 20 min and analyzed cold-stable microtubules. HURP localized to cold-stable microtubules (Fig. 4D, top), which was disrupted by HURP depletion (Fig. 4D bottom), consistent with the previous study (Sillje et al., 2006).

We next depleted importin-β and analyzed its effects on HURP and K-fibers (Fig. 4E, S4D). Importin-β depletion caused a remarkable relocalization of HURP from K-

fibers near chromosomes to spindle microtubules (Fig. 4E-F). Although K-fiber localization of HURP was unclear in importin-β depleted cells due to the relative accumulation of HURP on spindle microtubules around spindle poles (Fig. 4E bottom), HURP was clearly detected on cold-stable K-fibers in importin-β depleted cells (Fig. 4G). These results suggest that HURP acts for K-fiber stabilization independently of importin-β.

HURP and importin-β localize throughout the spindle in RanGAP1-depleted cells

Whereas HURP and importin-β have different roles for K-fiber stabilization (Fig. 4D, G), both proteins accumulate at K-fibers near chromosomes downstream of RCC1 (Fig. 3C-D). To comprehensively understand mechanisms of Ran-based spatial regulation of HURP and importin-β, we next analyzed the behaviors of HURP and importin-β in RanGAP1-depleted cells, in which Ran-GTP should exist throughout cells. RanGAP1 degradation did not cause clear phenotypes in spindle length (Fig. 4H-I, Fig. S4E). However, both HURP and importin-β localized throughout the spindle with increased intensities in RanGAP1-depleted cells (Fig. 4H-I, Fig. S4F). These results suggest that HURP and importin-β behave together and preferentially interact with microtubules in the presence of Ran-GTP (Fig. 4J).

RCC1 is required to maintain HURP's K-fiber localization during metaphase

Based on our results, we constructed a revised model for the control of spindle assembly downstream of the Ran-GTP gradient (Fig. 4J). In this model, importin-β

globally inhibits HURP's microtubule-biding activity by masking HURP's 2nd microtubule-binding domain (MTBD2) (Sillje et al., 2006; Song et al., 2014), and the chromosome-derived Ran-GTP gradient locally dissociates HURP from importin-β resulting in the activation of HURP near chromosomes (Fig. 4J). In this model, Ran-GTP and importin-β underlie a dynamic cycle of HURP's microtubule binding and dissociation near chromosomes. To test this model and whether this is valid after the spindle has already assembled, we next sought to acutely degrade RCC1 during metaphase by combining AID-mediated degradation with APC/C inhibitors (Fig. 5A). Cells were synchronized in G2 using RO-3306 (Vassilev et al., 2006) and released in the medium containing the APC/C inhibitors, Apcin and proTAME (Sackton et al., 2014), to arrest cells at metaphase without inhibiting the proteasome. RCC1-mAC signals were reduced to undetectable level by 60-90 min following the addition of IAA under metaphase-arrested condition (Fig. 5B). In the presence of RCC1, HURP-mCherry accumulated on K-fibers near chromosomes (Fig. 5B, t = -5 and 30). In contrast, following the degradation of RCC1, HURP weakly localized throughout the spindle (Fig. 5B, t= 60 and 90). Interestingly, spindle length was not substantially affected during this process (Fig. 5B-C, compare t = -5 with t = 60 min), suggesting that K-fiber stabilization by HURP contributes to spindle length regulation primarily during prometaphase. Together, these results support our model (Fig. 4J) and further indicate that the Ran-based network dynamically maintains HURP's K-fiber localization even after the spindle is assembled.

Discussion

NuMA acts for spindle-pole focusing independently of the Ran-importin network in cultured human cells

In the prevailing models (Fig. 1A), all SAFs including NuMA, TPX2, and HURP are expected to be similarly regulated by the chromosome-derived Ran-GTP gradient (Chang et al., 2017). However, SAFs localize and function at different locations on the spindle: NuMA accumulates around spindle poles distant from chromosomes (Fig.1C), whereas HURP localizes to K-fibers near chromosomes (Fig.3C, Fig. 6). Consistent with this distinct spatial localization, we demonstrated that the Ran-based network is dispensable for the localization and functions of NuMA (Fig. 1C-G, Fig. 2D-G), but is indispensable for HURP (Fig. 3C, 4E, 4H), in mitotic human cells. Considering mitotic arrest and abnormal spindle phenotypes caused by TPX2 depletion (Garrett et al., 2002; Kufer et al., 2002) (T.K. unpublished results), majority of TPX2 would also be functional even in the absence of Ran-GTP in mitotic human cells (Fig. 3B). Although we do not exclude the possibility that Ran-GTP liberates NuMA and TPX2 from importin-β near chromosomes, this contribution must be very minor in mitotic human cells. In mitotic cells, centrosomes act as a major microtubule-nucleation sites and recruit multiple signaling molecules including kinases. Other parallel pathways derived from centrosomes may act to liberate NuMA from inhibitory importins and make the Ran-GTP gradient dispensable for NuMA in mitosis. From this point of view, NuMA may be more potently regulated by Ran-GTP in human oocyte, in which Ran-GTP plays a dominant role in assembling meiotic spindle independently of centrosomes (Holubcova et al., 2015).

The Ran-based network dynamically polarizes and maintains HURP on K-fibers near chromosomes

In contrast to NuMA, we demonstrated that HURP is dynamically regulated by the Ran-based network in mitotic human cells (Fig. 3C, 4E, H). Although HURP has been identified previously as a downstream target of Ran-GTP (Sillje et al., 2006), we found that HURP additionally colocalizes with importin-β on K-fibers near chromosomes (Fig. S1K, Fig. 4A, E), and acts for K-fiber stabilization independently of importin-β (Fig. 4D, G). In addition, we demonstrated that HURP is dynamically maintained on K-fibers after spindle assembly downstream of Ran-GTP (Fig. 5B). Based on our results, we propose a local cycling model for the establishment and maintenance of HURP's polarized localization to spindle microtubules (Fig. 6). After nuclear envelope break down (NEBD), HURP strongly interacts with microtubules through its two microtubule binding domains (MTBD1 and MTBD2) (Sillje et al., 2006; Song et al., 2014) (Fig. 6-a). Importin-β binds to the HURP on microtubules, and then dissociates HURP from the microtubules (Fig. 6-b) because importin-β masks HURP's 2nd microtubule binding domain (MTBD2) (Song et al., 2014). However, in the vicinity of chromosomes, chromosome-derived Ran-GTP releases HURP from importin-β (Sillje et al., 2006) (Fig. 6-c), and the liberated HURP quickly interacts with microtubules around chromosomes (Fig.6-d). As importin-β is diffusively localized throughout cells (Fig. 4A, E), importin-β again binds and dissociates the HURP from microtubules near chromosomes (Fig. 6-e), but Ran-GTP again releases HURP from importin-β (Fig. 6-c). By repeating this local binding-dissociation cycle (Fig 6 c-d-e), HURP, but not importin-β, would act to stabilize microtubules and

generates stable K-fibers (Fig. 4D, G). This dynamic property would be suitable for bundling short microtubules nucleated around kinetochores (Sikirzhytski et al., 2018) and for coupling HURP's polarized localization with microtubule flux on the mitotic spindle.

A new toolkit and mitosis-specific degradation assays to dissect mitotic roles of Ran-importin network

To define mitotic functions of the Ran-based network, it is critical to inactivate the network specifically during mitosis due to its central role in nuclear-cytoplasmic transport during interphase. Previously, tsBN2, a temperature-sensitive RCC1 mutant hamster cell line (Nishimoto et al., 1978), and a small molecule inhibitor, importazole (Soderholm et al., 2011), have been developed to acutely inhibit functions of RCC1 or importin-β, respectively. Here, we established three human cell lines for RCC1, RanGAP1 and importin-β using AID technology (Natsume et al., 2016), that allowed us to systematically deplete the Ran-Importin network in human cells. Importantly, by combining nocodazole or APC/C inhibitors, we succeeded in degrading the Ran-based network specifically in prometaphase (Fig. 2C-F) or metaphase (Fig. 5A-B), respectively. Given that spindle length was virtually unaffected by RCC1 degradation at metaphase (Fig. 5B-C), HURP-based K-fiber stabilization would act during prometaphase to define proper spindle length. Because there are many other mitotic proteins regulated downstream of Ran-GTP (Forbes et al., 2015; Kiyomitsu and Cheeseman, 2012; Kiyomitsu and Cheeseman, 2013), these AID-cell lines will be useful to dissect these downstream functions. In addition, as this AID-mediated mitotic

352 degradation can be applicable for other multi-functional proteins such as dynein and
353 NuMA (Natsume et al., 2016; Okumura et al., 2018), these new assays will further
354 provide novel insights into mechanisms and roles of spindle assembly and maintenance
355 in animal cells.
356

Acknowledgments

We thank I. M. Cheeseman for critical reading of the manuscript, R. Inaba, and K. Murase for technical assistance. This work was supported by grants from PRESTO program (JPMJPR13A3) of the Japan Science and Technology agency (JST) for T.K, a Career Development Award of the Human Frontier Science Program (CDA00057/2014-C) for T.K., KAKENHI (16K14721 and 17H05002 for T.K, 17H01431 for G.G.) of the Japan Society for Promotion of Science (JSPS), NIG-JOINT (2014B-B-3, 2015-A1-19, 2016-A1-22 for T.K.) of National Institute of Genetics (NIG), and the Naito Foundation for T.K.

Author contributions

Conceptualization, T.K ; Investigation, T.K., K.T., H.H., M.N., and M.O ; Formal analysis, T.K and K.T ; Methodology, T.K. and M.K ; Writing, T.K ; Supervision, T.K and G.G ; Funding Acquisition, T.K., M.K and G.G.

Declaration of interests

The authors declare no competing interests.

Materials and methods

- Plasmid Construction

  Plasmids for CRISPR/Cas9-mediated genome editing and auxin-inducible degron were constructed according to the protocol described in Natsume et al., (Natsume et al., 2016) and Okumura et al., (Okumura et al., 2018). To construct donor plasmids containing homology arms for RCC1 (~500-bp homology arms), RanGAP1 (~500-bp arms), importin-β (~500-bp homology arms), HURP (~200-bp homology arms), and TPX2 (~200-bp homology arms), gene synthesis services from Eurofins Genomics K.K. (Tokyo, Japan) or Genewiz (South Plainsfield, NJ) were used for RCC1 and others, respectively. Plasmids and sgRNA sequences used in this study are listed in Supplementary Tables S1 and S2, and will be deposited to Addgene.

- Cell Culture, Cell Line Generation and Antibodies

  HCT116 cells were cultured as described previously (Okumura et al., 2018). Knock-in cell lines were generated according to the procedures described in Okumura et al., (Okumura et al., 2018). To activate the auxin-inducible degradation, cells were treated with 2 μg/mL Dox and 500 μM indoleacetic acid (IAA) for 20–24 h. Cells with undetectable signals for mAID-fusion proteins were analyzed. The cell lines and primers used in this study are listed in Tables S1 and S3, respectively.

  Antibodies against tubulin (DM1A, Sigma-Aldrich, 1:2,000), NuMA (Abcam, 1:1,000), RCC1 (Cell Signaling Technology, D15H6, Rabbit mAb, 1:100), RanGAP1 (Santa Cruz Biotechnology, H-180, 1:200), importin-β (GeneTex, 3E9 Mouse mAb, 1:100), and HURP (E. Nigg laboratory, 1 : 200) were used for western blotting. For RCC1 immunoblots, the membrane was incubated with the anti-RCC1 antibody overnight at 4 °C.

- Microscope System

  Imaging was performed using spinning-disc confocal microscopy with a 60× 1.40 numerical aperture objective lens (Plan Apo λ, Nikon, Tokyo, Japan). A CSU-W1 confocal unit (Yokogawa Electric Corporation, Tokyo, Japan) with five lasers (405, 488, 561, 640, and 685 nm, Coherent, Santa Clara, CA) and an ORCA-Flash4.0 digital CMOS camera (Hamamatsu Photonics, Hamamatsu City, Japan) were attached to an ECLIPSE Ti-E inverted microscope (Nikon) with a perfect focus system. DNA images in Figure 2A/B or Figure 4D/G were obtained using either SOLA LED light engine (Lumencor, Beaverton, OR) or 405 nm laser, respectively.

- Immunofluorescence and Live Cell Imaging

  For immunofluorescence in Figure S1K, HURP-mACF cells were fixed with PBS containing 3% paraformaldehyde and 2% sucrose for 10 min at room temperature. Fixed cells were permeabilized with 0.5% Triton X-100™ for 5 min on ice, and pretreated with PBS containing 1% BSA for 10 min at room temperature after washing with PBS. Importin-β was visualized using the anti-importin-β antibody (1:500). Images of multiple z-sections were acquired by spinning-disc confocal microscopy using 0.5-μm spacing and camera binning 2. Maximally projected images from 3 z-sections were shown.

For live cell imaging, cells were cultured on glass-bottomed dishes (CELLview™, #627860 or #627870, Greiner Bio-One, Kremsmünster, Austria) and maintained in a stage-top incubator (Tokai Hit, Fujinomiya, Japan) to maintain the same conditions used for cell culture (37 °C and 5% CO_2). In most cases, three to five z-section images using 0.5-μm spacing were acquired and single z-section images were shown, unless otherwise specified. Microtubules was stained with 50 nM SiR-tubulin or SiR700-tubulin (Spirochrome) for >1 h prior to image acquisition. DNA was stained with 50 ng/mL Hoechst® 33342 (Sigma-Aldrich) or 20 nM SiR-DNA (Spirochrome) for > 1 h before observation. To visualize SNAP-tagged HURP in Fig. 4E, cells were incubated with 0.1 μM TMR-Star (New England BioLabs) for > 2 h, and TMR-Star were removed before observation. To optimize image brightness, same linear adjustments were applied using Fiji and Photoshop.

- Prometaphase degradation assay and nocodazole washout
  To degrade mAID-tagged proteins during nocodazole arrest, cells were treated with 2 μg/mL Dox and 3.3 μM nocodazole at the indicated times (Fig. 2C). Five hours after the addition of nocodazole, cell culture dishes were moved to the stage of a microscope equipped with a peristaltic pump (SMP-21S, EYELA, Tokyo Rikakikai). Two z-section images were acquired using 2 μm spacing at three different (X.Y) positions and at 5 min intervals, with 500 μM IAA added during the first interval. After 90 min, the nocodazole-containing medium was completely replaced with fresh medium using the peristaltic pump at a velocity of 20 sec/ml for 15 min. Images were acquired for a further 2 h and maximum intensity projection images are shown in Figure 2D-F.

- Metaphase degradation assay
  To degrade mAID-tagged proteins in metaphase-arrested cells, the cells were treated with 50 μM Apcin (I-444, Boston Biochem) and 20 μM proTAME (I-440, Boston Biochem) at the indicated times (Fig. 5A). Three z-section images were acquired using 1 μm spacing at six different (X.Y) positions and at 5 min intervals, with 500 μM IAA added during the first interval. Maximum intensity projection images are shown in Figure 5B.

- Cold treatment assay
  To increase the number of cells in metaphase, cells were treated with 20 μM MG132 (C2211, Sigma-Aldrich) for 90 min. To visualize SNAP-tagged HURP (Fig. 4G), cells were incubated with 0.1 μM TMR-Star (S9105S, New England BioLabs) for at least 30 min. Before fixation, cells were incubated in ice-cold medium for 20 min (Sillje et al., 2006) to depolymerize non-kinetochore microtubules.

- Statistical Analysis
  To determine the significance of differences between the mean values obtained for two experimental conditions, Welch's *t*-tests (Prism 6; GraphPad Software, La Jolla, CA) or a Z-test for proportions (Allto Consulting, Leeds, UK) were used as indicated in the figure legends.

468 **Table S1: Cell lines used in this study.**

No.	Name	Description	Clone No.	Plasmids used	Parental cell	Reference
1	HCT116 tet-OsTIR1	AAVS1::PTRE3G OsTIR1 (Puro)		pAAVS1 T2 and MK243 (Addgene#72835)		(Natsume et al., 2016)
2	RCC1-mAC	AAVS1::PTRE3G OsTIR1 (Puro), RCC1:: RCC1-mAID-mClover (Neo)	1	pTK361+ pHH45	1	This study
3	RCC1-mAC + NuMA-mCh	AAVS1::PTRE3G OsTIR1 (Puro), RCC1:: RCC1-mAID-mClover (Neo), NuMA1:: NuMA-mCh (Hygro)	1	pTK372+ pTK435	2	This study
4	RanGAP1-mAC	AAVS1::PTRE3G OsTIR1 (Puro), RanGAP1:: RanGAP1-mAID-mClover (Neo)	9	pHH49 + pHH51	1	This study
5	RanGAP1-mAC + NuMA-mCh	AAVS1::PTRE3G OsTIR1 (Puro), RanGAP1:: RanGAP1-mAID-mClover (Neo), NuMA1:: NuMA-mCh (Hygro)	5	pTK372+ pTK435	4	This study
6	importin-β-mAC	AAVS1::PTRE3G OsTIR1 (Puro), importin-β:: importin-β-mAID-mClover (Neo)	7	pHH50 + pHH57	1	This study
7	importin-β-mAC + NuMA-mCh	AAVS1::PTRE3G OsTIR1 (Puro), importin-β:: importin-β-mAID-mClover (Neo), NuMA1:: NuMA-mCh (Hygro)	1	pTK372+ pTK435	6	This study
8	RCC1-mAC + importin-β-mCh	AAVS1::PTRE3G OsTIR1 (Puro), RCC1:: RCC1-mAID-mClover (Neo), NuMA1:: NuMA-mCh (Hygro)	6	pHH50 +pTK481	2	This study
9	RCC1-mAC + HURP-mCh	AAVS1::PTRE3G OsTIR1 (Puro), RCC1:: RCC1-mAID-mClover (Neo), HURP:: HURP-mCh (Hygro)	8	pTK532+ pTK541	2	This study
10	RCC1-mAC + TPX2-mCh	AAVS1::PTRE3G OsTIR1 (Puro), RCC1:: RCC1-mAID-mClover (Neo), TPX2:: TPX2-mCh (Hygro)	1	pTK527+ pTK502	2	This study
11	RanGAP1-mAC + HURP-mCh	AAVS1::PTRE3G OsTIR1 (Puro), RanGAP1:: RanGAP1-mAID-mClover (Neo), HURP:: HURP-mCh (Hygro)	5	pTK532+ pTK541	4	This study
12	RanGAP1-mAC + importin-β-mCh	AAVS1::PTRE3G OsTIR1 (Puro), RanGAP1:: RanGAP1-mAID-mClover (Neo), importin-β:: importin-β-mCh (Hygro)	12	pHH50 +pTK481	4	This study
13	importin-β-mAC + HURP-SNAP	AAVS1::PTRE3G OsTIR1 (Puro), importin-β:: importin-β-mAID-mClover (Neo), HURP:: HURP-SNAP (Hygro)	3	pTK532+ pTK589	6	This study
14	HURP-mACF	AAVS1::PTRE3G OsTIR1 (Puro), HURP:: HURP-mAID-mClover-3FLAG (Neo)	13	pTK532+ pTK596	1	This study
15	HURP-mACF + importin-β-mCh	AAVS1::PTRE3G OsTIR1 (Puro), HURP:: HURP-mAID-mClover-3FLAG (Neo), importin-β:: importin-β-mCh (Hygro)	14	pHH50 +pTK481	14	This study

469
470

471 **Table S2: sgRNA sequences for CRISPR/Cas9-mediated genome editing**

Gene locus	sgRNA (5'-3')	PAM	Plasmid Name
NuMA1 (C-terminus)	gtggggccactcactggtac	tgg	pTK372 (Okumura et al., 2018)
RCC1 (C-terminus)	gactgtatgctggcccccgc	tgg	pTK361
RanGAP1 (C-terminus)	tctgctgcagacgctgtaca	agg	pHH49
importin-β (C-terminus)	agttcgagccgccgcccgaa	agg	pHH50
HURP	caaaattctcctggttgtag	agg	pTK532
TPX2	tgcggataccgcccggcaat	ggg	pTK527

472

473 **Table S3: PCR primers to confirm gene editing**

Gene	Primer sequence	Primer name	Figures
RCC1	gaatgccattccaggcag	oHH88	Figure S1A
RCC1	ttctgcacgttcctctgg	oHH89	Figure S1A
NUMA1	gagcctcaaagaaggccc	oTK542	Figure S1B, S1E, S1H
NUMA1	agcaggaaccagggcctac	oTK566	Figure S1B, S1E, S1H
RanGAP1	gctgccgcaggaccagggcttggtg	oHH93	Figure S1D
RanGAP1	attccctggcctatgtctgctggaa	oHH94	Figure S1D
HURP	ctcttgatggatactttactg	oTK749	Figure S3B, S4A, S4D, S4F
HURP	cccttgagaaagagtatatcta	oTK750	Figure S3B, S4A, S4D, S4F
importin-β	ggagtaaggagttttgagagtatcg	oHH97	Figure S1G, S3C, S4C, S4F
importin-β	aaatcttctctagagctaggcaacg	oHH98	Figure S1G, S3C, S4C, S4F
TPX2	tctgacatccctctcactg	oTK660	Figure S3A
TPX2	ggagtctaatcgagacattc	oTK661	Figure S3A

474

475

References

Beaven, R., R.N. Bastos, C. Spanos, P. Rome, C.F. Cullen, J. Rappsilber, R. Giet, G. Goshima, and H. Ohkura. 2017. 14-3-3 regulation of Ncd reveals a new mechanism for targeting proteins to the spindle in oocytes. *J Cell Biol*. 216:3029-3039.

Bennabi, I., M.E. Terret, and M.H. Verlhac. 2016. Meiotic spindle assembly and chromosome segregation in oocytes. *J Cell Biol*. 215:611-619.

Bischoff, F.R., C. Klebe, J. Kretschmer, A. Wittinghofer, and H. Ponstingl. 1994. RanGAP1 induces GTPase activity of nuclear Ras-related Ran. *Proc Natl Acad Sci U S A*. 91:2587-2591.

Bischoff, F.R., and H. Ponstingl. 1991. Catalysis of guanine nucleotide exchange on Ran by the mitotic regulator RCC1. *Nature*. 354:80-82.

Chang, C.C., T.L. Huang, Y. Shimamoto, S.Y. Tsai, and K.C. Hsia. 2017. Regulation of mitotic spindle assembly factor NuMA by Importin-beta. *J Cell Biol*. 216:3453-3462.

Ciciarello, M., R. Mangiacasale, C. Thibier, G. Guarguaglini, E. Marchetti, B. Di Fiore, and P. Lavia. 2004. Importin beta is transported to spindle poles during mitosis and regulates Ran-dependent spindle assembly factors in mammalian cells. *J Cell Sci*. 117:6511-6522.

Compton, D.A., I. Szilak, and D.W. Cleveland. 1992. Primary structure of NuMA, an intranuclear protein that defines a novel pathway for segregation of proteins at mitosis. *J Cell Biol*. 116:1395-1408.

Dumont, J., S. Petri, F. Pellegrin, M.E. Terret, M.T. Bohnsack, P. Rassinier, V. Georget, P. Kalab, O.J. Gruss, and M.H. Verlhac. 2007. A centriole- and RanGTP-independent spindle assembly pathway in meiosis I of vertebrate oocytes. *J Cell Biol*. 176:295-305.

Forbes, D.J., A. Travesa, M.S. Nord, and C. Bernis. 2015. Reprint of "Nuclear transport factors: global regulation of mitosis". *Curr Opin Cell Biol*. 34:122-134.

Furuta, M., T. Hori, and T. Fukagawa. 2016. Chromatin binding of RCC1 during mitosis is important for its nuclear localization in interphase. *Mol Biol Cell*. 27:371-381.

Gaglio, T., A. Saredi, and D.A. Compton. 1995. NuMA is required for the organization of microtubules into aster-like mitotic arrays. *J Cell Biol*. 131:693-708.

Garrett, S., K. Auer, D.A. Compton, and T.M. Kapoor. 2002. hTPX2 is required for normal spindle morphology and centrosome integrity during vertebrate cell division. *Curr Biol*. 12:2055-2059.

Goshima, G., and J.M. Scholey. 2010. Control of mitotic spindle length. *Annu Rev Cell Dev Biol*. 26:21-57.

Gruss, O.J., R.E. Carazo-Salas, C.A. Schatz, G. Guarguaglini, J. Kast, M. Wilm, N. Le Bot, I. Vernos, E. Karsenti, and I.W. Mattaj. 2001. Ran induces spindle assembly by reversing the inhibitory effect of importin alpha on TPX2 activity. *Cell*. 104:83-93.

Hasegawa, K., S.J. Ryu, and P. Kalab. 2013. Chromosomal gain promotes formation of a steep RanGTP gradient that drives mitosis in aneuploid cells. *J Cell Biol*. 200:151-161.

Heald, R., and A. Khodjakov. 2015. Thirty years of search and capture: The complex simplicity of mitotic spindle assembly. *J Cell Biol*. 211:1103-1111.

Holubcova, Z., M. Blayney, K. Elder, and M. Schuh. 2015. Human oocytes. Error-prone chromosome-mediated spindle assembly favors chromosome segregation defects in human oocytes. *Science*. 348:1143-1147.

Hueschen, C.L., S.J. Kenny, K. Xu, and S. Dumont. 2017. NuMA recruits dynein activity to microtubule minus-ends at mitosis. *Elife*. 6.

Joseph, J., S.H. Tan, T.S. Karpova, J.G. McNally, and M. Dasso. 2002. SUMO-1 targets RanGAP1 to kinetochores and mitotic spindles. *J Cell Biol*. 156:595-602.

Kalab, P., and R. Heald. 2008. The RanGTP gradient - a GPS for the mitotic spindle. *J Cell Sci*. 121:1577-1586.

Kalab, P., A. Pralle, E.Y. Isacoff, R. Heald, and K. Weis. 2006. Analysis of a RanGTP-regulated gradient in mitotic somatic cells. *Nature*. 440:697-701.

Kiyomitsu, T. 2019. The cortical force-generating machinery: how cortical spindle-pulling forces are generated. *Curr Opin Cell Biol*. 60:1-8.

Kiyomitsu, T., and I.M. Cheeseman. 2012. Chromosome- and spindle-pole-derived signals generate an intrinsic code for spindle position and orientation. *Nat Cell Biol*. 14:311-317.

Kiyomitsu, T., and I.M. Cheeseman. 2013. Cortical dynein and asymmetric membrane elongation coordinately position the spindle in anaphase. *Cell*. 154:391-402.

Kufer, T.A., H.H. Sillje, R. Korner, O.J. Gruss, P. Meraldi, and E.A. Nigg. 2002. Human TPX2 is required for targeting Aurora-A kinase to the spindle. *J Cell Biol*. 158:617-623.

Mogessie, B., K. Scheffler, and M. Schuh. 2018. Assembly and Positioning of the Oocyte Meiotic Spindle. *Annu Rev Cell Dev Biol*. 34:381-403.

Moore, W., C. Zhang, and P.R. Clarke. 2002. Targeting of RCC1 to chromosomes is required for proper mitotic spindle assembly in human cells. *Curr Biol*. 12:1442-1447.

Moutinho-Pereira, S., N. Stuurman, O. Afonso, M. Hornsveld, P. Aguiar, G. Goshima, R.D. Vale, and H. Maiato. 2013. Genes involved in centrosome-independent mitotic spindle assembly in Drosophila S2 cells. *Proc Natl Acad Sci U S A*. 110:19808-19813.

Nachury, M.V., T.J. Maresca, W.C. Salmon, C.M. Waterman-Storer, R. Heald, and K. Weis. 2001. Importin beta is a mitotic target of the small GTPase Ran in spindle assembly. *Cell*. 104:95-106.

Natsume, T., T. Kiyomitsu, Y. Saga, and M.T. Kanemaki. 2016. Rapid Protein Depletion in Human Cells by Auxin-Inducible Degron Tagging with Short Homology Donors. *Cell Rep*. 15:210-218.

Nishimoto, T., E. Eilen, and C. Basilico. 1978. Premature of chromosome condensation in a ts DNA- mutant of BHK cells. *Cell*. 15:475-483.

Okumura, M., T. Natsume, M.T. Kanemaki, and T. Kiyomitsu. 2018. Dynein-Dynactin-NuMA clusters generate cortical spindle-pulling forces as a multi-arm ensemble. *Elife*. 7.

Petry, S. 2016. Mechanisms of Mitotic Spindle Assembly. *Annu Rev Biochem*. 85:659-683.

Sackton, K.L., N. Dimova, X. Zeng, W. Tian, M. Zhang, T.B. Sackton, J. Meaders, K.L. Pfaff, F. Sigoillot, H. Yu, X. Luo, and R.W. King. 2014. Synergistic blockade of mitotic exit by two chemical inhibitors of the APC/C. *Nature*. 514:646-649.

Sikirzhytski, V., F. Renda, I. Tikhonenko, V. Magidson, B.F. McEwen, and A. Khodjakov. 2018. Microtubules assemble near most kinetochores during early prometaphase in human cells. *J Cell Biol*. 217:2647-2659.

Silk, A.D., A.J. Holland, and D.W. Cleveland. 2009. Requirements for NuMA in maintenance and establishment of mammalian spindle poles. *J Cell Biol*. 184:677-690.

Sillje, H.H., S. Nagel, R. Korner, and E.A. Nigg. 2006. HURP is a Ran-importin beta-regulated protein that stabilizes kinetochore microtubules in the vicinity of chromosomes. *Curr Biol*. 16:731-742.

Soderholm, J.F., S.L. Bird, P. Kalab, Y. Sampathkumar, K. Hasegawa, M. Uehara-Bingen, K. Weis, and R. Heald. 2011. Importazole, a small molecule inhibitor of the transport receptor importin-beta. *ACS Chem Biol*. 6:700-708.

Song, L., A. Craney, and M. Rape. 2014. Microtubule-dependent regulation of mitotic protein degradation. *Mol Cell*. 53:179-192.

Tang, T.K., C.J. Tang, Y.J. Chao, and C.W. Wu. 1994. Nuclear mitotic apparatus protein (NuMA): spindle association, nuclear targeting and differential subcellular localization of various NuMA isoforms. *J Cell Sci*. 107 (Pt 6):1389-1402.

Vassilev, L.T., C. Tovar, S. Chen, D. Knezevic, X. Zhao, H. Sun, D.C. Heimbrook, and L. Chen. 2006. Selective small-molecule inhibitor reveals critical mitotic functions of human CDK1. *Proc Natl Acad Sci U S A*. 103:10660-10665.

Walczak, C.E., and R. Heald. 2008. Mechanisms of mitotic spindle assembly and function. *Int Rev Cytol*. 265:111-158.

Wiese, C., A. Wilde, M.S. Moore, S.A. Adam, A. Merdes, and Y. Zheng. 2001. Role of importin-beta in coupling Ran to downstream targets in microtubule assembly. *Science*. 291:653-656.

Yesbolatova, A., T. Natsume, K.I. Hayashi, and M.T. Kanemaki. 2019. Generation of conditional auxin-inducible degron (AID) cells and tight control of degron-fused proteins using the degradation inhibitor auxinole. *Methods*.

Zierhut, C., and H. Funabiki. 2015. Nucleosome functions in spindle assembly and nuclear envelope formation. *Bioessays*. 37:1074-1085.

Figure 1

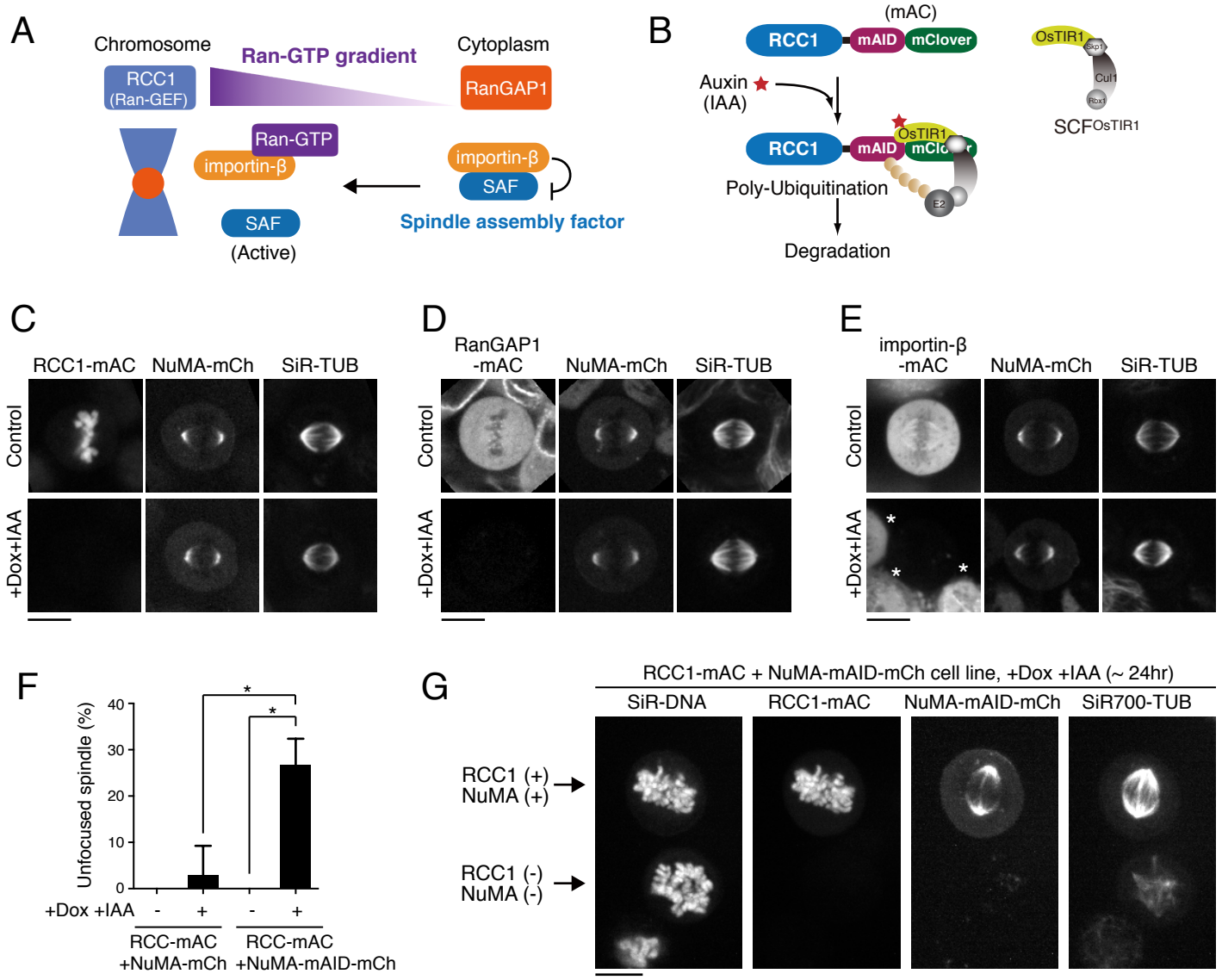

Figure 1. NuMA localizes at spindle poles and acts for spindle-pole focusing independently of RCC1.
(A) The prevailing model of the mitotic spindle assembly regulated by Ran-related factors.
(B) Schematic of the auxin-inducible degradation (AID) system.
(C-E) Metaphase RCC1-mAC (C), RanGAP1-mAC (D) or importin-β-mAC cells (E) showing live fluorescent images of mAC-tagged proteins, NuMA-mCherry (mCh), and SiR-TUB after 24 h following Dox and IAA treatment. * in E indicates cells with importin-β signals in the presence of Dox and IAA.
(F) Quantification of RCC1-mAC (n = 27, 34) or RCC1-mAC + NuMA-mAID-mCh (n = 37, 113) cells with unfocused spindles in the presence or absence of Dox and IAA, respectively. Bars indicate the mean ± SEM of >4 independent experiments. * indicates statistical significance as determined by Welch's t-test ($p < 0.05$).
(G) Live fluorescent images of SiR-DNA, RCC1-mAC, NuMA-mAID-mCherry, and SiR700-TUB in RCC1-mAC and NuMA-mAID-mCh double knock-in cells following 24 h of Dox and IAA treatment. Two cells with or without RCC1 and NuMA signals were analyzed in the same field. Eight z-section images were acquired using 1.0 μm spacing and maximum intensity projection images are shown. Scale bars = 10 μm.

Figure 2

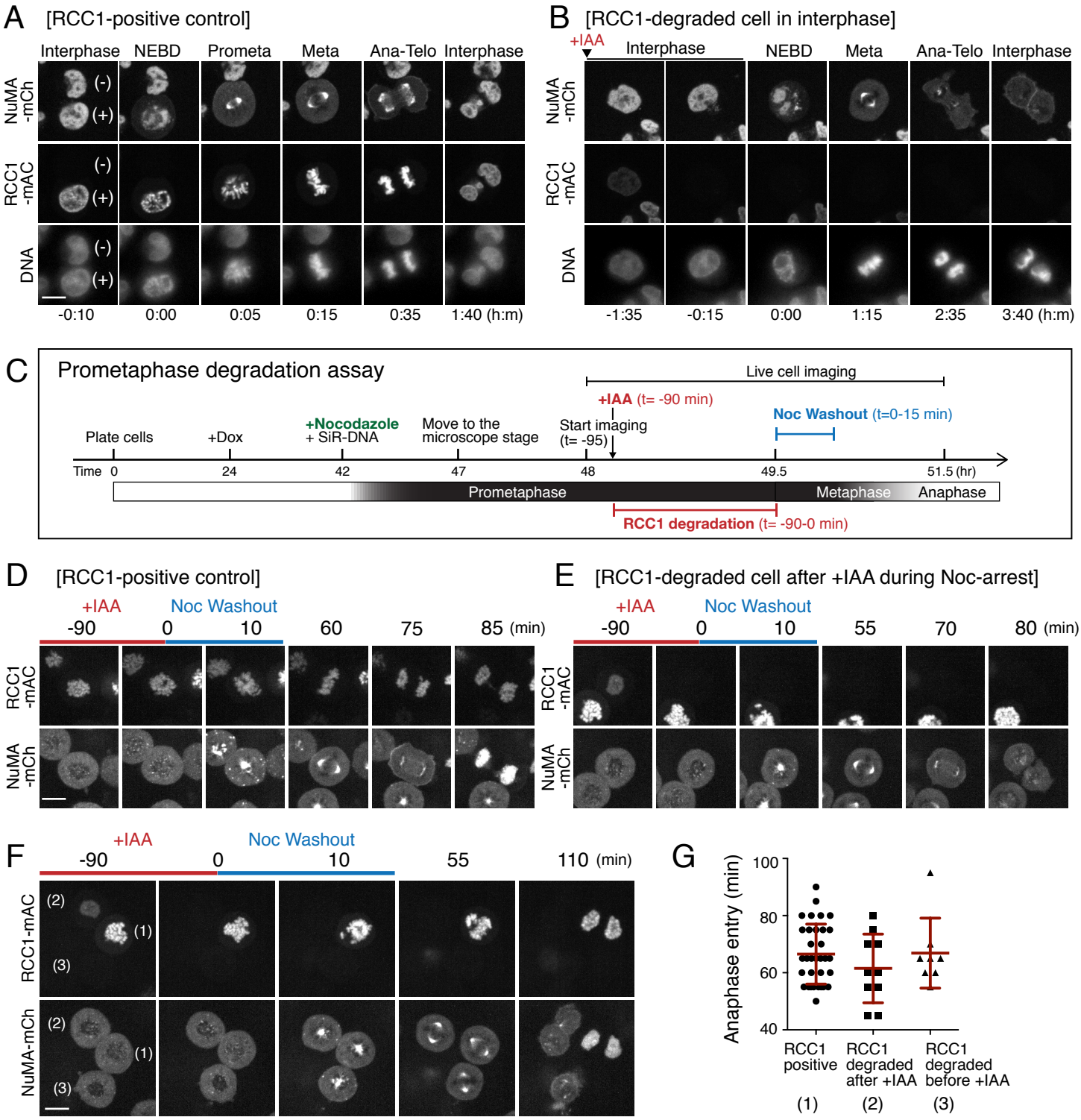

Figure 2. Acute RCC1 degradation during prometaphase does not substantially affect localization and function of NuMA at the spindle poles.

(A-B) Live fluorescent images of NuMA-mCh, RCC1-mAC, and DNA (Hoechst 33342 staining) in RCC1-mAC positive (A) and RCC1-depleted (B) cells. Following 21 h of Dox treatment, auxin (IAA) was added and cells were imaged for 6 h. RCC1-positive and -depleted cells are indicated by (+) or (-), respectively, in A. The RCC1 signal was reduced to an undetectable level following IAA treatment during interphase in B. Two z-section images were acquired using 2 µm spacing and single z-section images are shown.

Figure 2

(C) Schematic diagram of the prometaphase degradation assay. Following Dox treatment, a high dose of nocodazole (3.3 μM) was added for 6 h to completely disrupt the mitotic spindle and arrest cells in prometaphase. IAA was then added for 90 min (indicated by the red line) to degrade RCC1 during mitosis. Nocodazole was washed away for 15 min (indicated by the light blue line) to initiate mitotic spindle assembly.
(D-E) Live fluorescent images of NuMA-mCh and RCC1-mAC in RCC1 positive (D) and RCC1-depleted cells after IAA treatment (E).
(F) Live fluorescent images of NuMA-mCh and RCC1-mAC in three different cells. RCC1 was not degraded in the cell (1), whereas RCC1-mAC was degraded in the cell (2) or (3) after or before IAA treatment, respectively. A cell identical to (E) is shown as the cell (2) to compare the phenotypes of the three different cell types in the same field.
(G) Scatterplots of anaphase entry time in RCC1 positive cells (66.5 ± 10.5, n = 33), RCC1-depleted cells after IAA treatment (61.5 ± 12.0, n = 10), and RCC1-depleted cells before IAA treatment (66.9 ± 12.2, n = 8). Bars indicate the mean ± SD of > 3 independent experiments. Scale bars = 10 μm..

Figure 3

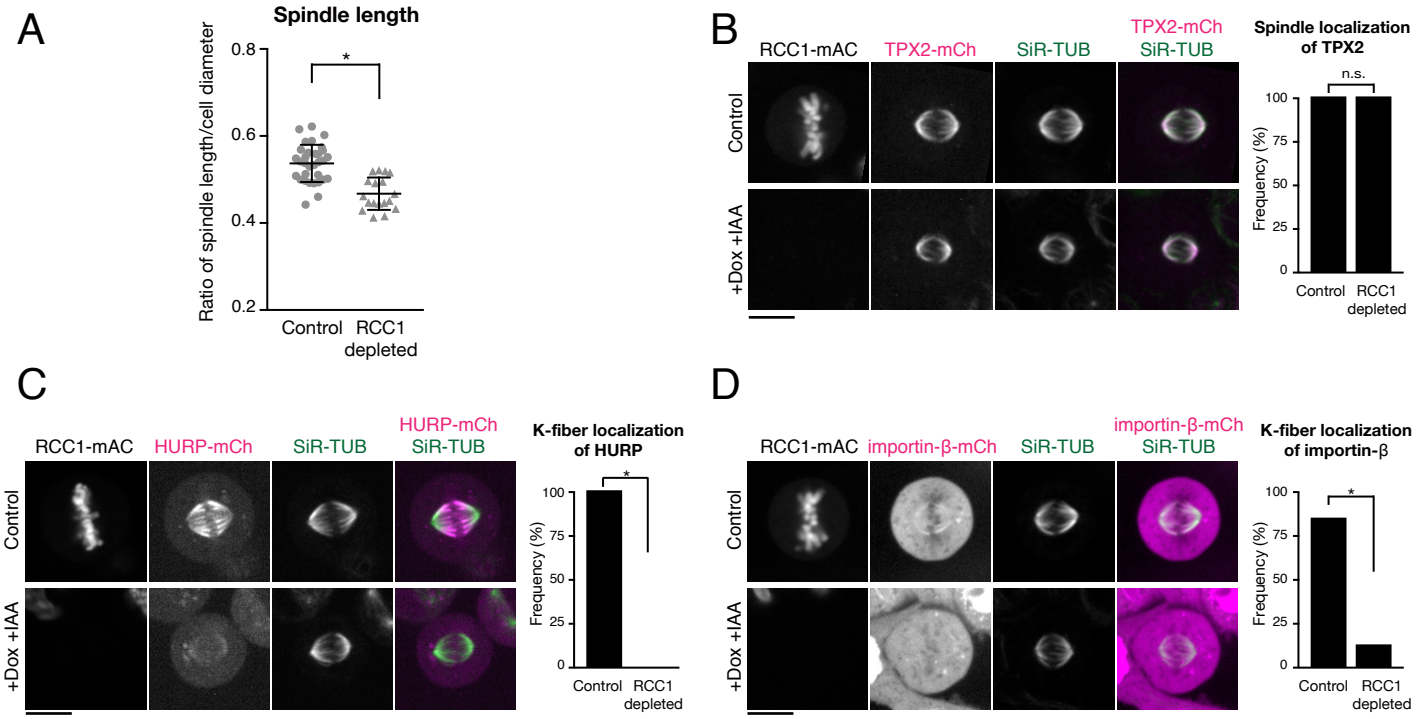

Figure 3. RCC1 regulates kinetochore-fiber localization of HURP and importin-β.
(A) Scatterplots of the ratio of spindle length and cell diameter in control (0.54 ± 0.04, n = 32) and RCC1-depleted (0.47 ± 0.04, n = 23) cells. Bars indicate mean ± SD from >3 independent experiments. * indicates statistical significance according to Welch's t-test ($p < 0.0001$).
(B-D) Left: Metaphase RCC1-mAC cells showing live fluorescent images of RCC1-mAC, SiR-TUB and TPX2-mCh (B), HURP-mCh (C), and importin-β-mCh (D) after 24 h following treatment with Dox and IAA. Right: Quantification of spindle or K-fiber localization of TPX2, HURP, or importin-β in control (n > 40) and RCC1-depleted (n > 40) cells from 3 independent experiments. * indicates statistical significance according to Z-test (99.9% confidence interval). Scale bars = 10 μm.

Figure 4

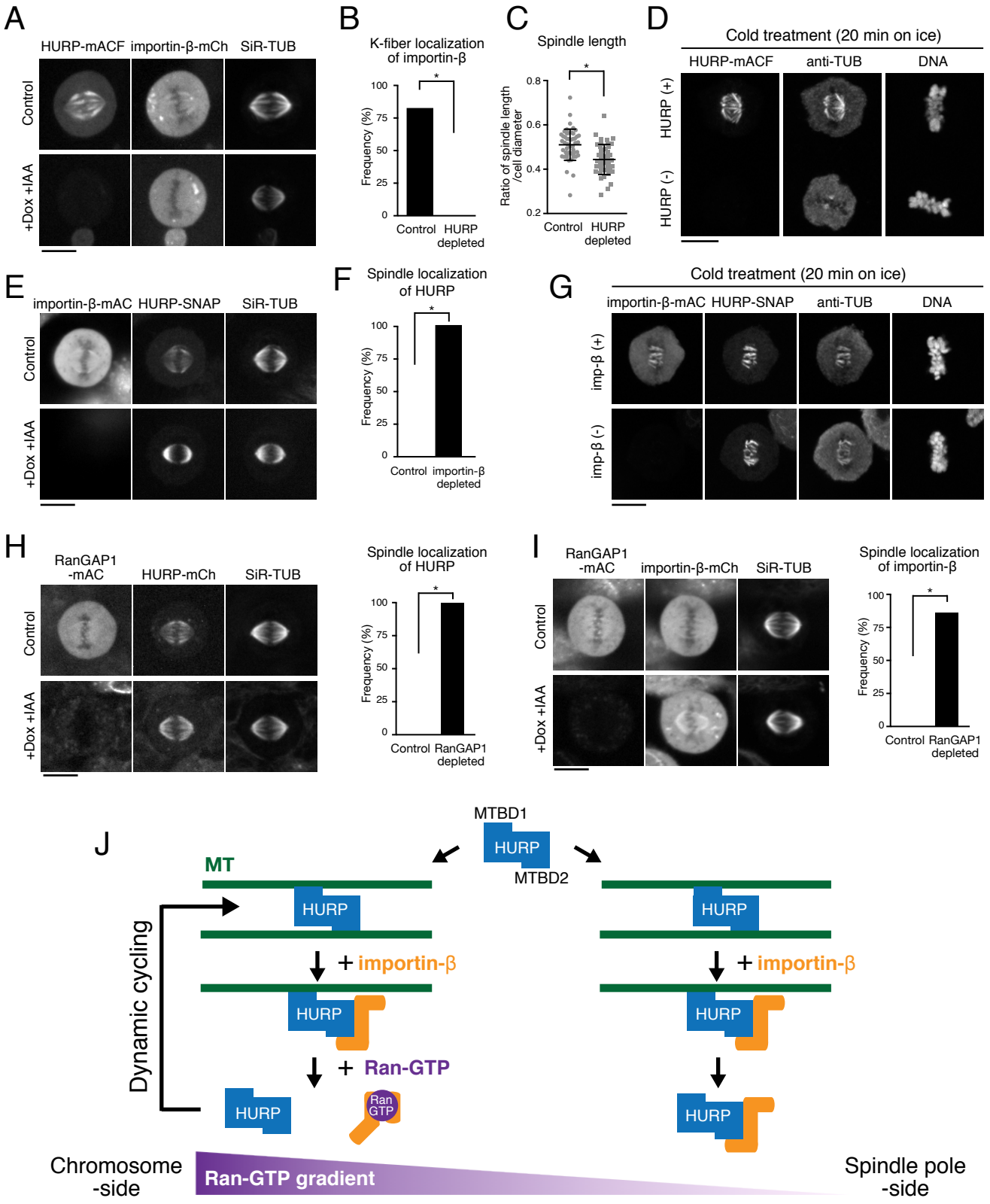

Figure 4. HURP, but not importin-β, is required to stabilize K-fibers.

(A) Metaphase HURP-mACF cells showing live fluorescent images of HURP-mACF, importin-β-mCh and SiR-TUB after 24 hrs following Dox and IAA treatment.

(B) Quantification of K-fiber localization of importin-β in control (n = 49) and HURP-depleted (n = 46) cells from 3 independent experiments. * indicates statistical significance according to Z-test (99.9% confidence interval).

(C) Scatterplots of the ratio of spindle length and cell diameter in control (0.64 ± 0.05, n = 49) and HURP-depleted (0.52 ± 0.06, n = 43) cells. * indicates statistical significance according to Welch's t-test ($p < 0.0001$).

(D) Fluorescent images of HURP-mACF, TUB, and DNA (Hoechst 33342 staining) in metaphase fixed cells treated with ice-cold medium for 20 min. Two cells with or without HURP signals were analyzed in the same field.

Figure 4

(E) Metaphase importin-β-mAC cells showing live fluorescent images of importin-β-mAC, HURP-SNAP and SiR-TUB after 24 h following treatment with Dox and IAA.
(F) Quantification of spindle localization of HURP in control (n = 49) and importin-β-depleted (n = 43) cells from 3 independent experiments. * indicates statistical significance according to Z-test (99.9% confidence interval).
(G) Fluorescent images of importin-β-mAC, HURP-SNAP, TUB, and DNA (Hoechst 33342 staining) in metaphase fixed cells treated with ice-cold medium for 20 min. Five z-section images were obtained using 0.5 μm spacing and maximum intensity projection images are shown in (D) and (G).
(H-I) Left: metaphase RanGAP1-mAC cells showing live fluorescent images of RanGAP1-mAC, SiR-TUB and HURP-mCh (H) or importin-β-mCh (I) after 24 h following Dox and IAA treatment. Right: quantification of K-fiber localization of HURP or importin-β in control (n = 45) and RanGAP1-depleted (n > 45) cells from 3 independent experiments. * indicates statistical significance according to Z-test (99.9% confidence interval). (J) A local cycling model of HURP on K-fibers regulated by Ran-GTP and importin-β. See text for details. Scale bars = 10 μm.

Figure 5

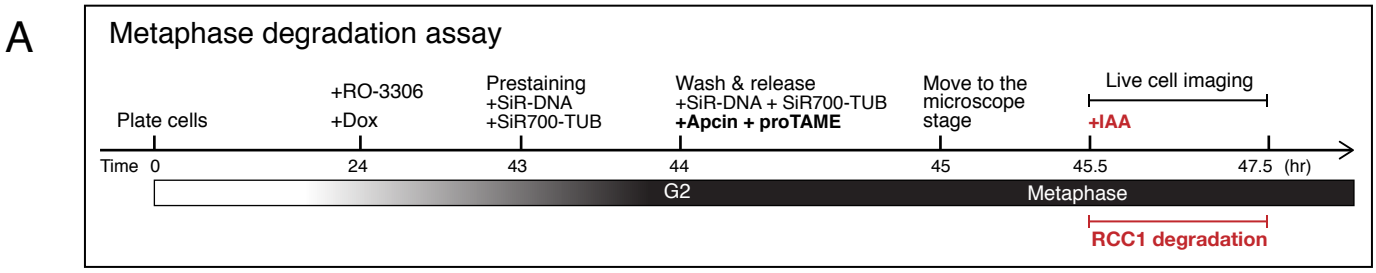

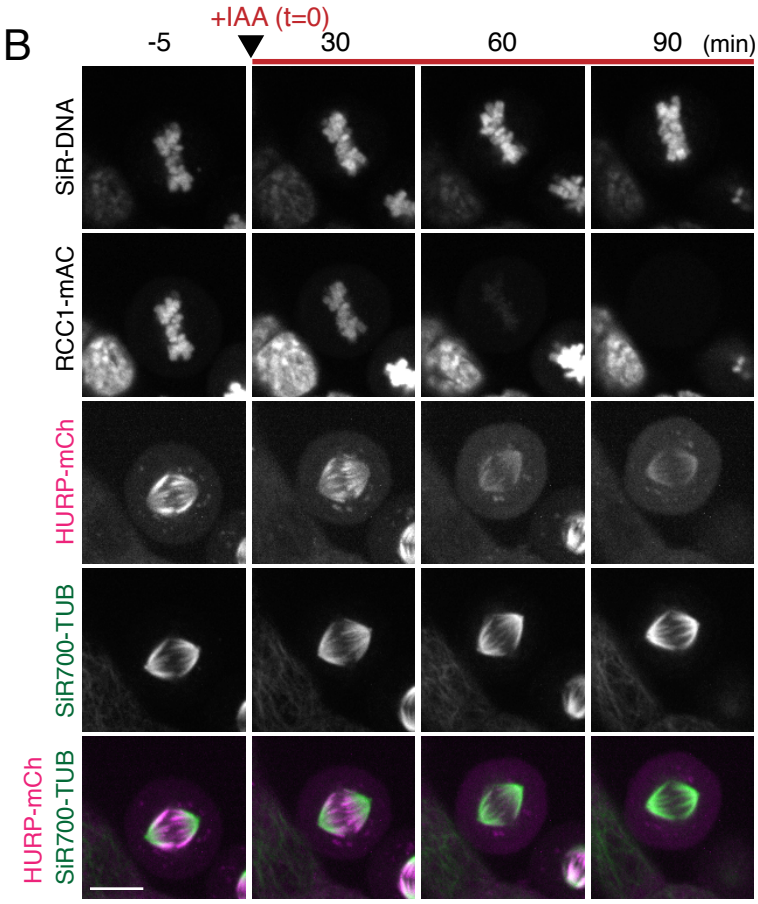

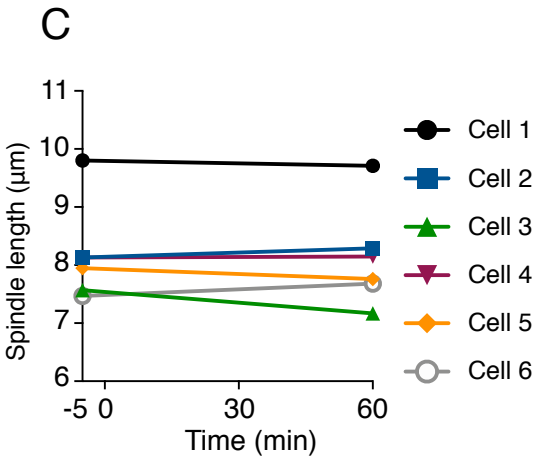

Figure 5. RCC1 is required to maintain HURP K-fiber accumulation during metaphase.
(A) Schematic diagram of the metaphase degradation assay. Following release from RO-3336-mediated G2 arrest, proTAME and Apcin were added to arrest the cells in metaphase. Auxin (IAA) was added (indicated by the red line) to induce RCC1 degradation during metaphase.
(B) Live fluorescent images of SiR-DNA, RCC1-mAC, NuMA-mCh, and SiR700-TUB showing acute auxin-mediated RCC1 degradation in metaphase-arrested cells.
(C) Spindle length measurement (n = 6) at t = -5 and 60 min in (B). Scale bar = 10 µm.

Figure 6

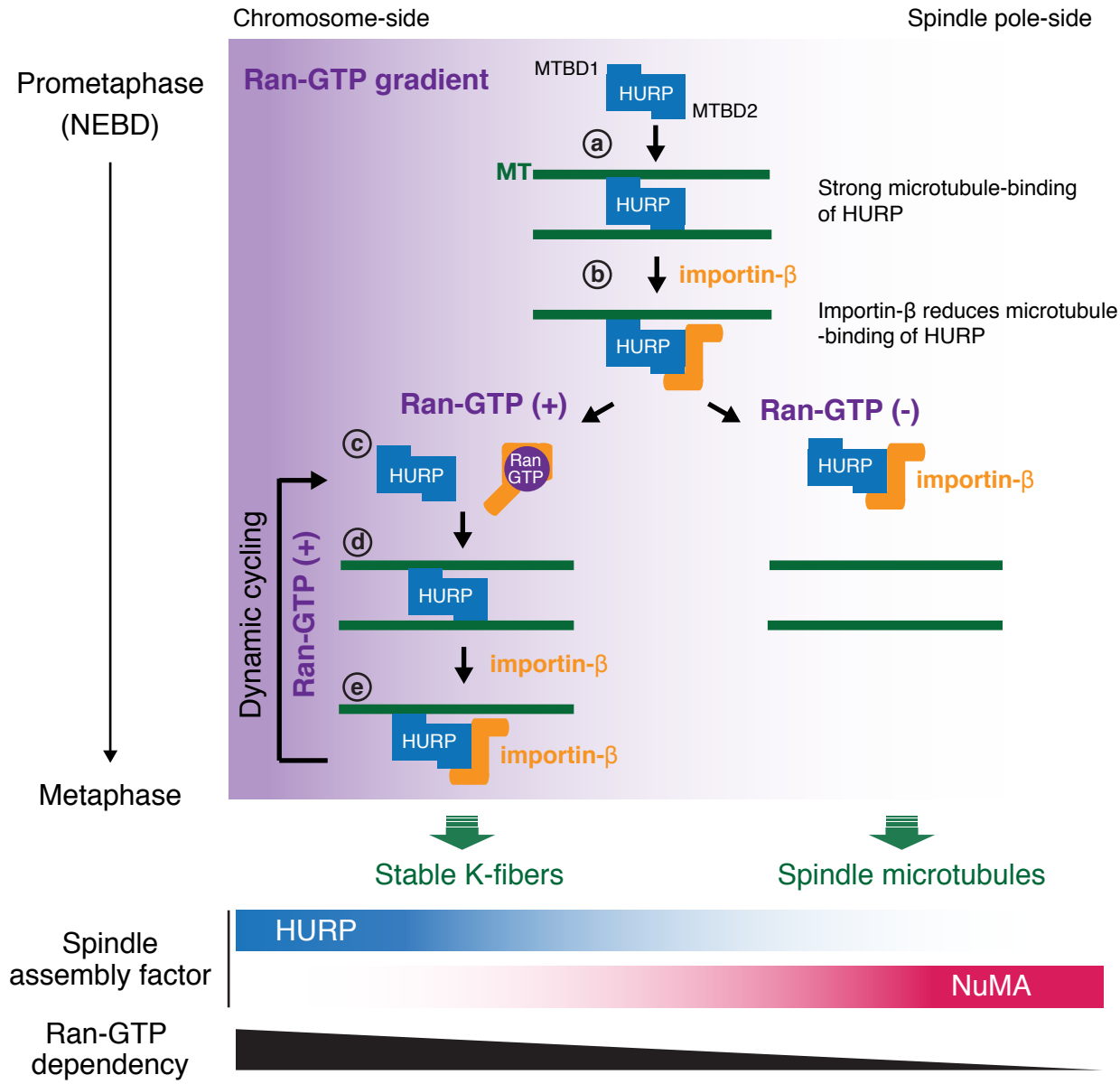

Figure 6. A local cycling model for the polarization and maintenance of HURP on K-fibers near chromosomes.

In the vicinity of chromosomes, Ran-GTP and importin-β promote the microtubule binding and dissociation cycle of HURP (c-d-e), resulting in stable HURP-dependent K-fiber formation. Chromosome-derived Ran-GTP regulates the localization of HURP on K-fibers, but not the localization and function of NuMA at the spindle poles in mitotic human cells. See text for details.

Supplemental Figure S1

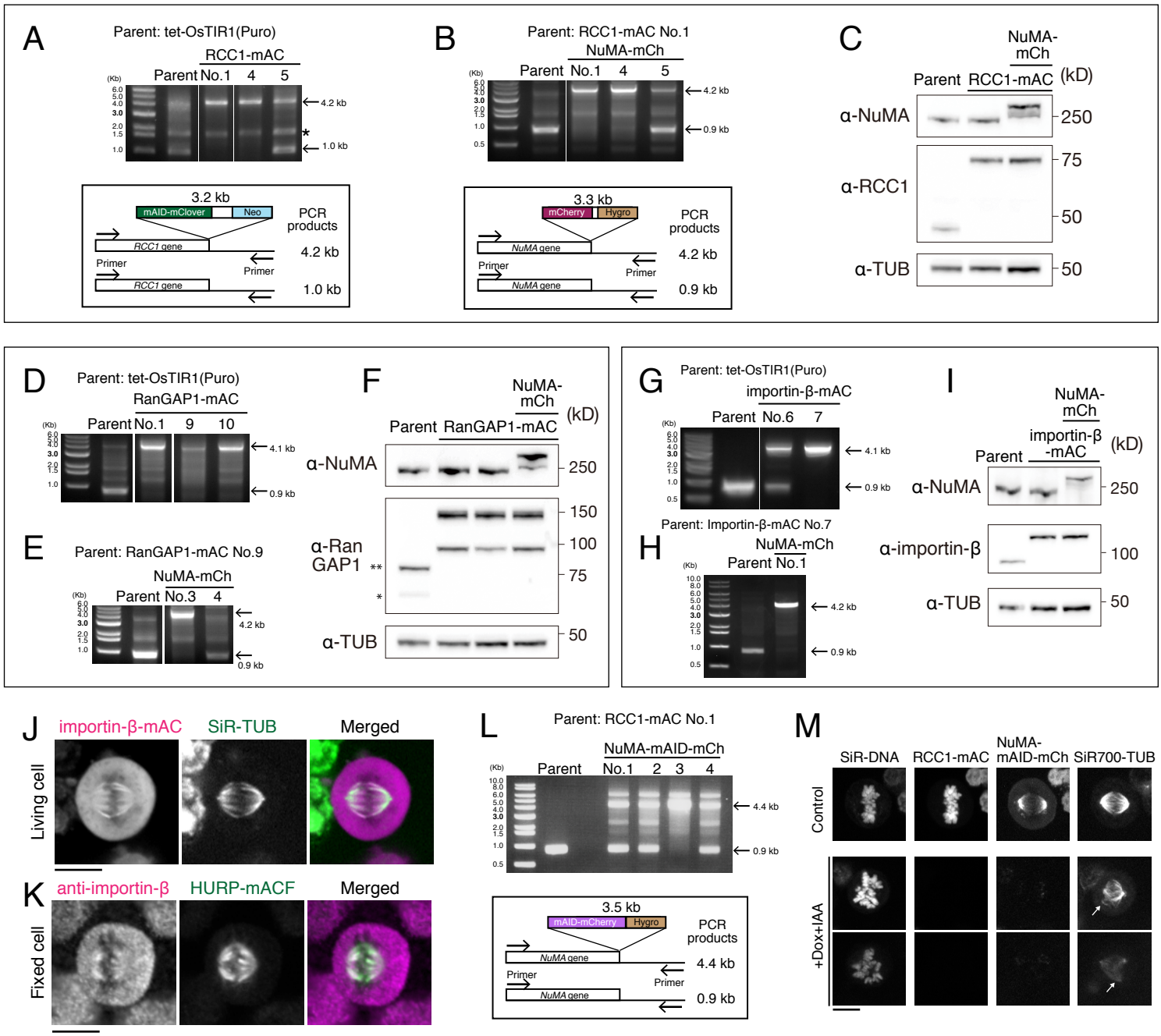

Figure S1. Generation of cell lines for auxin-induced degradation of endogenous RCC1, RanGAP1, and importin-β.

(A) Genomic PCR showing clone genotypes after neomycin (Neo) selection. Clone No.1 was used as a parental cell in the second selections. * indicates a non-specific band.

(B) Genomic PCR showing clone genotypes after hygromycin (Hygro) selection. Clone No.1 was used in this study.

(C) Immunoblotting for anti-NuMA, anti-RCC1 and anti-α-tubulin (TUB, loading control) showing bi-allelic insertion of the indicated tags.

(D) Genomic PCR showing clone genotypes after neomycin (Neo) selection. The clone No.9 was used as a parental cell in the second selections.

(E) Genomic PCR showing clone genotypes after hygromycin (Hygro) selection. The clones No.3 was selected for further use.

(F) Immunoblotting for anti-NuMA, anti-RanGAP1 and anti-α-tubulin (TUB, loading control) showing bi-allelic insertion of the indicated tags. * and ** indicate RanGAP1 and SUMO-1 conjugated RanGAP1, respectively.

(G) Genomic PCR showing clone genotypes after neomycin (Neo) selection. The clone No.7 was used as a parental cell in the second selections.

(H) Genomic PCR showing clone genotype after hygromycin (Hygro) selection. Clone No.1 was selected for further use.

(I) Western blot detection using anti-NuMA, anti-importin-β and anti-α-tubulin antibodies (TUB, loading control) showing bi-allelic insertion of the indicated tags.

(J) Metaphase importin-β-mAC cells showing live fluorescent images of importin-β-mAC, and SiR-TUB. Single z-section images are shown.

(K) Immunofluorescence images of fixed metaphase cells showing K-fiber localization of endogenous importin-β and mAID-tagged HURP (HURP-mACF). The maximally projected images from 3 z-sections are shown.

(L) Genomic PCR showing clone genotype after hygromycin (Hygro) selection. Clone No.3 was selected for further use.

(M) Live fluorescent images of SiR-DNA, RCC1-mAC, NuMA-mAID-mCh, and SiR-TUB. A spindle-pole focusing defect (indicated by the arrow in panel 2) and abnormal spindle formation (panel 3) were observed in RCC1-mAC and NuMA-mAID-mCh co-depleted cells 20-24 h after Dox and IAA treatment. Five z-section images were acquired using 1.0 μm spacing and maximum intensity projection images are shown. Scale bars = 10 μm.

Supplemental Figure S2

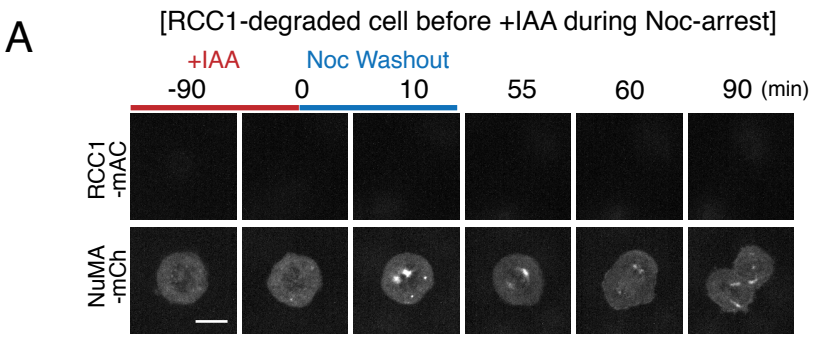

Figure S2. Phenotypes of RCC1-degraded cells following nocodazole washout.
(A) Live fluorescent images of NuMA-mCh and RCC1-mAC in an RCC1-depleted cell. RCC1 was degraded during nocodazole arrest and before IAA treatment due to basal OsTIR1 activity; however, NuMA localized to the spindle poles and the RCC1-degraded cell exited mitosis as observed in RCC1-positive cells. Two z-section images were acquired using 2 µm spacing and maximal intensity projection images are shown. Scale bar = 10 µm.

Supplemental Figure S3

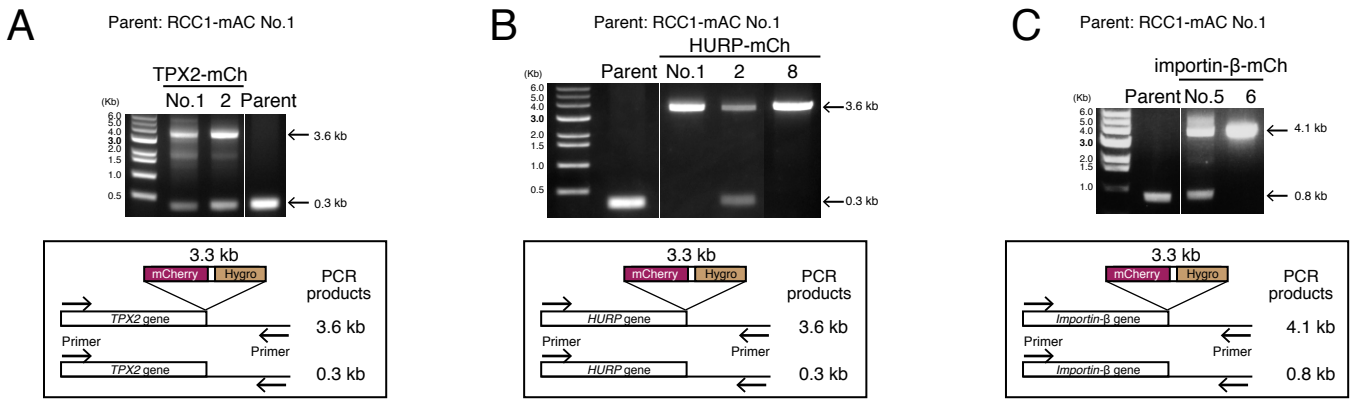

Figure S3. Generation of double knock-in cell lines that express RCC1-mAC and mCherry-fuzed TPX2, HURP, or importin-β.
(A-C) Genomic PCRs showing clone genotypes after hygromycin (Hygro) selections. Clones No.1 (A), No. 8 (B), and No.6 (C) were used. The mCherry cassette was inserted into only one copy of TPX2 gene loci (A).

Supplemental Figure S4

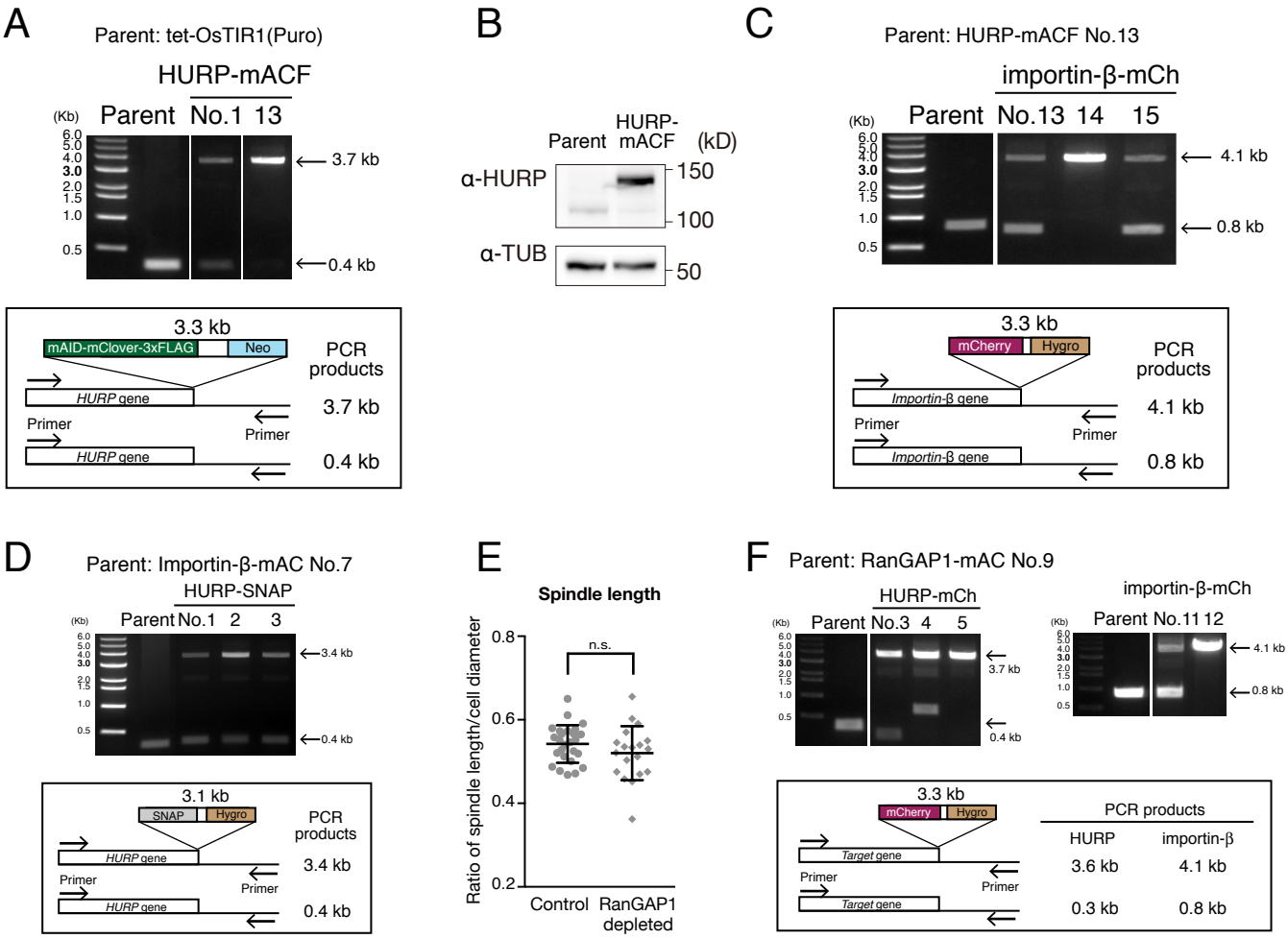

Figure S4. Generation of cell lines that degrade or visualize endogenous HURP.
(A) Genomic PCR showing clone genotype after neomycin (Neo) selection. Clone No.13 was used as a parental cell in the second selections.
(B) Immunoblotting for anti-HURP and anti-α-tubulin (TUB, loading control) showing bi-allelic insertion of the indicated tags.
(C-D) Genomic PCR showing clone genotypes after hygromycin (Hygro) selection. Clone No.14 (C) and No. 3 (D) were used, respectively. The SNAP cassette was inserted into only one copy of HURP gene loci (D).
(E) Scatterplots of the ratio of spindle length and cell diameter in control (0.54 ± 0.04, n = 26) and RanGAP1-depleted (0.52 ± 0.07, n = 19) cells. Bars indicate mean ± SD from >3 independent experiments. The differences were not statistically significant based on Welch's t-test in C ($p = 0.2108$).
(F) Genomic PCR showing clone genotypes after hygromycin (Hygro) selection. The clones No.5 (HURP-mCh), and No.12 (importin-β-mCh) were used, respectively.